Journal of Glaciology



Article

Cite this article: Lv M, Quincey DJ, Guo H, King O, Liu G, Yan S, Lu X, Ruan Z (2020). Examining geodetic glacier mass balance in the eastern Pamir transition zone. *Journal of Glaciology* **66**(260), 927–937. https://doi.org/10.1017/jog.2020.54

Received: 13 December 2019
Revised: 27 June 2020
Accepted: 29 June 2020
First published online: 3 August 2020

Key words:
Digital elevation model; eastern Pamir; glacier mass balance; surge-type glaciers

Author for correspondence:
Mingyang Lv, E-mail: lmynju@163.com

© The Author(s), 2020. Published by Cambridge University Press. This is an Open Access article, distributed under the terms of the Creative Commons Attribution licence (http://creativecommons.org/licenses/by/4.0/), which permits unrestricted re-use, distribution, and reproduction in any medium, provided the original work is properly cited.

cambridge.org/jog

Examining geodetic glacier mass balance in the eastern Pamir transition zone

Mingyang Lv[1,2,3], Duncan J. Quincey[3], Huadong Guo[1,2], Owen King[4], Guang Liu[2], Shiyong Yan[5], Xiancai Lu[1] and Zhixing Ruan[2]

[1]School of Earth Sciences and Engineering, Nanjing University, Nanjing, China; [2]Key Laboratory of Digital Earth Science, Aerospace Information Research Institute, Chinese Academy of Sciences, Beijing, China; [3]School of Geography, University of Leeds, Leeds, UK; [4]School of Geography and Sustainable Development, University of St Andrews, St Andrews, Scotland and [5]School of Environment Science and Spatial Informatics, China University of Mining and Technology, Xuzhou, China

Abstract

Glaciers in the eastern Pamir have reportedly been gaining mass during recent decades, even though glaciers in most other regions in High Mountain Asia have been in recession. Questions still remain about whether the trend is strengthening or weakening, and how far the positive balances extend into the eastern Pamir. To address these gaps, we use three different digital elevation models to reconstruct glacier surface elevation changes over two periods (2000–09 and 2000–15/16). We characterize the eastern Pamir as a zone of transition from positive to negative mass balance with the boundary lying at the northern end of Kongur Tagh, and find that glaciers situated at higher elevations are those with the most positive balances. Most (67% of 55) glaciers displayed a net mass gain since the 21st century. This led to an increasing regional geodetic glacier mass balance from -0.06 ± 0.16 m w.e. a^{-1} in 2000–09 to 0.06 ± 0.04 m w.e. a^{-1} in 2000–15/16. Surge-type glaciers, which are prevalent in the eastern Pamir, showed fluctuations in mass balance on an individual scale during and after surges, but no statistical difference compared to non-surge-type glaciers when aggregated across the region.

Introduction

Fluctuations in mountain glaciers are recognized as a key indicator of climate change, resulting in sea-level changes and regional glacier-related hazards (Oerlemans, 1994; Meier and others, 2007; Bolch and others, 2012; Gardner and others, 2013; IPCC, 2019). High Mountain Asia (HMA), including the Tibetan Plateau and its surroundings, is home to the largest number of glaciers outside Earth's polar regions. Most of these glaciers have been in a sustained phase of recession during recent decades. The annual mass balance of glaciers in HMA was -0.18 ± 0.04 m w.e. a^{-1} from 2000 to 2016 (Brun and others, 2017), and in the Himalaya, the rate of ice loss almost doubled in 2000–16 (-0.43 ± 0.14 m w.e. a^{-1}) when compared to 1975–2000 (-0.22 ± 0.13 m w.e. a^{-1}) (Maurer and others, 2019). In the western part of HMA, however, it is generally recognized that glaciers behave abnormally (Gardelle and others, 2013; Kääb and others, 2015; Farinotti and others, 2020). In particular, glaciers in the eastern Pamir, the Kunlun Shan and the central Tibetan Plateau showed thickening of 0.1–0.7 m a^{-1} during the early part of the 21st century (Treichler and others, 2019). The Pamir has been highlighted in several studies as the zone of transition between negative (to the west) and positive (to the east) mass balances (Brun and others, 2017; Lin and others, 2017), differentiating the glaciers here from a worldwide thinning trend (Gardner and others, 2013; Zemp and others, 2017).

Most of the glacierized area in the eastern Pamir lies in the Kingata Mountains, the Kongur Tagh and the Muztag Ata (Fig. 1). Few detailed studies exist for these three ranges, but those that do are common in showing widespread glacier recession over the latter decades of the 20th century. Areal losses of $10.8 \pm 1.1\%$ were measured between 1963 and 2009 (Zhang and others, 2016b) and mass losses of -0.14 ± 0.24 m w.e. a^{-1} were recorded between 1971/76 and 1991 (Zhang and others, 2016a). However, since the 21st century, glaciers in the eastern Pamir began to gain mass again. From 2000 to 2014, the mass budget of the eastern Pamir was calculated as $+0.12 \pm 0.09$ m w.e. a^{-1} (Lin and others, 2017) and a slight expansion in glacier area ($+0.5 \pm 0.1$ km^2) was detected from 2009 to 2014 (Zhang and others, 2016a). On a more local scale, and focusing on the Muztag Ata in particular, a mass balance of $+0.04 \pm 0.27$ m w.e. a^{-1} was calculated by Holzer and others (2015) for the period 1999–2013. Although these disparate data go some way toward characterizing mass changes in the region, the transition between mass gain and mass loss is not well studied and glacier-specific data are still lacking. The rate of change in mass balance is also poorly characterized since the 21st century.

Glacier-specific mass-balance data are particularly important for this region because many of the glaciers are surge-type (Lv and others, 2016; Shangguan and others, 2016; Lv and others, 2019). The behavior of surge-type glaciers is known to depart significantly from climate-driven changes in mass balance that are conventionally associated with non-surge type (Bhambri and others, 2017). Glaciers that surge build-up large volumes of ice at high-elevation (albeit often

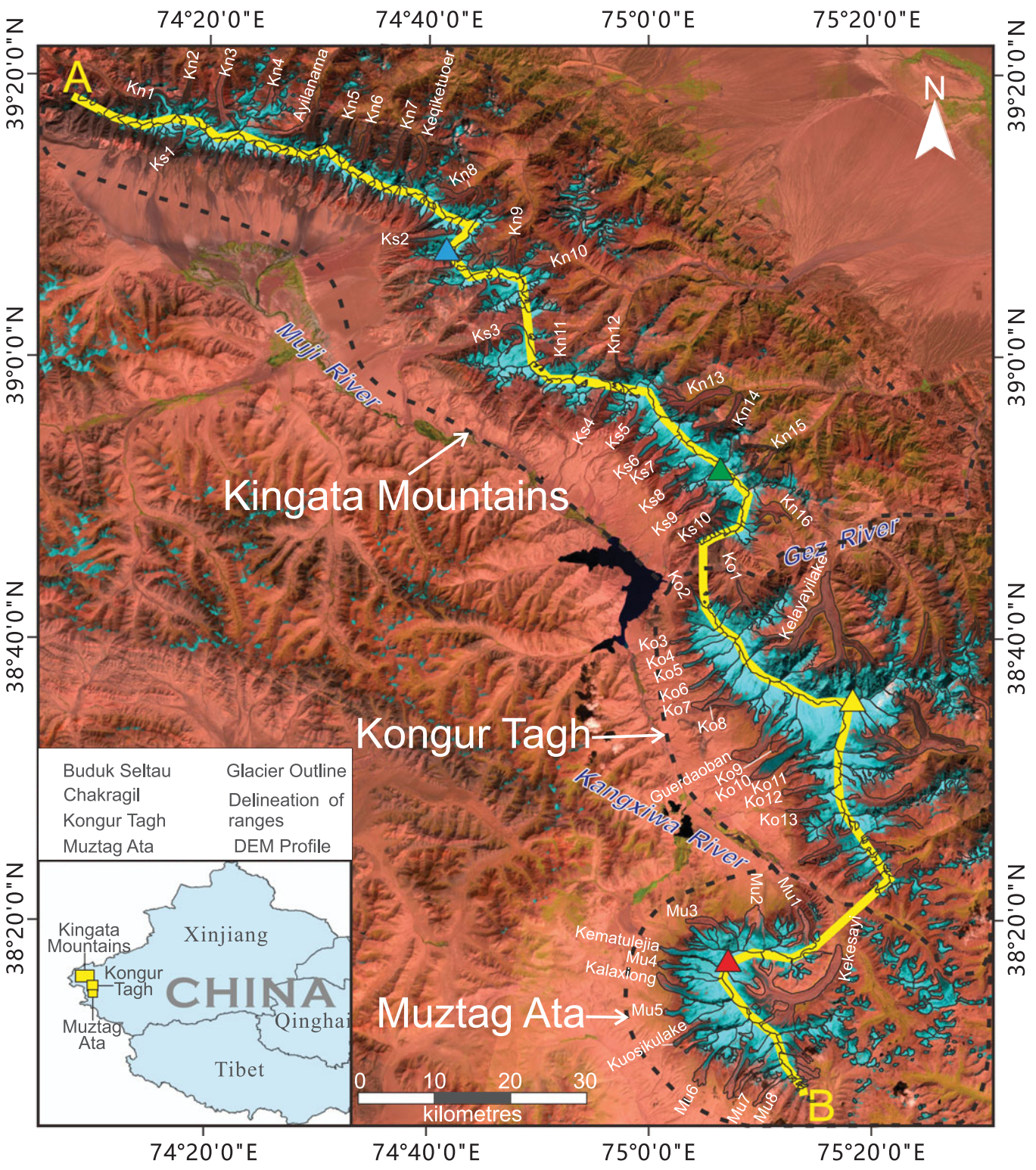


Fig. 1. The eastern Pamir, showing major mountain ranges, key rivers and the glaciers (labeled) assessed within this study. The background image was acquired by Landsat OLI (band combination of 6-5-4) on 9 September 2017. The DEM profile is shown in Figure 5.

still within the ablation area) for many decades, before rapidly discharging the mass down-glacier during short-lived surge events. Previous studies have indicated that during the active surge phase, the geodetic mass balance can be strongly negative (Aðalgeirsdóttir and others, 2005; Kochtitzky and others, 2019), but over longer (e.g. decadal) timescales, there appears to be little difference between the mass balances of surge-type and non-surge-type glaciers (Gardelle and others, 2013; Brun and others, 2017; Berthier and others, 2019). There remains some uncertainty, therefore, as to whether surge-enhanced ablation may impact on regional mass-balance calculations.

In this study, we use three different digital elevation model (DEM) datasets to reconstruct the surface elevation changes in the eastern Pamir over two periods (2000–09, 2000–15/16), to assess spatial and temporal changes in mass balance during the early part of 21st century. We characterize the location of the transition boundary and how mass balances either side of the boundary have evolved since the start of 21st century. We present

https://doi.org/10.1017/jog.2020.54 Published online by Cambridge University Press

a comparison of surge-type and non-surge-type glacier mass balances, and evaluate the extent to which the presence of surge-type glaciers may impact on broad-region mass budget estimations.

Study area

The eastern Pamir (38°N–39°N, 73°E–75°E) is located in western China and is sometimes recognized as the tail of the West Kunlun Shan. The topography in the eastern Pamir ranges from 3000 m a.s.l. to >7600 m a.s.l.. Kongur Tagh, with an elevation of 7649 m a.s.l., is the highest summit in the eastern Pamir. Muztag Ata is 7509 m a.s.l. and Chakragil, the highest peak of the Kingata Mountains, is 6727 m a.s.l. (Fig. 1). As one of the coldest and driest regions around the world, glaciers in this area are acknowledged to be of continental type (Zhang, 1980; Shangguan and others, 2006).

The eastern Pamir has a glacierized area of 2362.5 km^2 (comprising 2106 glaciers) (Mölg and others, 2018). Nearly 68% (1602.3 km^2) of this area is contained in the Kingata Mountains, the Kongur Tagh and the Muztag Ata. Large glaciers, often formed with multiple tributaries, are mostly located in the Kongur Tagh and Muztag Ata, while glaciers in the Kingata Mountains are smaller in size (Fig. 1). Many of the larger glacier tongues are covered by a continuous debris layer. Glacier meltwater in the eastern Pamir makes a substantial contribution to rivers such as the Muji, the Kangxiwa and the Gez, and is a critical natural resource for people living downstream (Liu and others, 2006).

The eastern Pamir is climatologically controlled by mid-latitude westerlies (Seong and others, 2009). Based on records from the Taxkogan meteorological station (37°46′N, 75°14′E; 3090.9 m a.s.l.), which is ~50 km south to the Muztag Ata, annual precipitation does not exceed 70 mm and the mean air temperature can be as high as 15°C between June and August (Shangguan and others, 2006). Since the 1950s, the mean summer temperature has increased by +0.7°C along with a slight increase in annual precipitation (Tian and others, 2006; Yao and others, 2012).

Data and methods

Digital elevation models

We calculated ice volume change with DEM differencing data in the study area and subsequently converted it to mass balance for each glacier. The Shuttle Radar Topography Mission (SRTM) 1 arc-second global DEM from 2000 provided the baseline dataset for the study. The NASA HMA 8 m DEM (Shean and others, 2016; Shean, 2017a, 2017b) provided the most recent elevation dataset. For a midpoint analysis, we generated eight DEMs from the Advanced Land Observing Satellite (ALOS) PRISM sensor (Table S1), complemented where necessary by a composite DEM derived from the same source (Tadono and others, 2014). The majority of the HMA and ALOS PRISM DEMs we analyzed were acquired toward the end of the ablation season (May to September in the Eastern Pamir).

SRTM 1 arc-second global DEM

The SRTM mission collected near-global data (57°S to 60°N) at 30 m-resolution in February 2000, using a C-band radar. This SRTM 1 arc-second global DEM (version 3.0) is provided by the United States Geological Survey (USGS) at Earth Gravitational Model 1996 orthometric heights and non-void-filled in our study area. The horizontal and vertical accuracies can be better than 10 m (Farr and others, 2007), although in areas of snow and ice, penetration of the radar signal has been shown to be problematic (Rignot and others, 2001). We used the SRTM 1 arc-second DEM (38°N–39°N, 74°E–75°E) as our reference elevation dataset during co-registration with two other elevation datasets, and performed corrections in snow-covered areas to account for potential subsurface penetration (detailed below).

ALOS-PRISM DEM and ALOS world 3D-30 m

ALOS-PRISM comprises three optical sensors with a spatial resolution of 2.5 m looking in backward, nadir and forward directions in order to measure precise land elevation (Tadono and others, 2009). We acquired eight sets of level-1B1 triplet mode scenes covering most of our study area captured between July and September 2009 (Table S1). We utilized the ERDAS IMAGINE Photogrammetry to extract the elevation data. We collected ground control points (GCPs) from fine-resolution imagery in Google Earth (provided by Digital Globe, NASA and Landsat/Copernicus), cross-checked against Landsat 8 images and SRTM DEM data to locate accurate horizontal and vertical positions. Tie-points were then automatically generated in IMAGINE Photogrammetry, and subsequently visually validated. Each scene was covered by at least 20 GCPs and between 30 and 40 tie points. ALOS PRISM DEMs were extracted at 30 m spatial resolution to match the SRTM DEM.

The ALOS World 3D-30 m (AW3D30) is a 30 m-resolution global digital elevation dataset released by the Japan Aerospace Exploration Agency in May 2015 using PRISM imagery acquired between 2006 and 2011. Though the AW3D30 presents an average elevation from all of the PRISM data acquired over this period, we used it to fill the gaps present in our self-generated PRISM DEMs, under the assumption that changes in elevation were consistent over this period. The metadata supporting the AW3D30 tiles indicate that up to five scenes were used to construct elevation values over the accumulation areas of the Muztag Ata, for example, yielding much better (and likely more robust) spatial coverage than a single image pair could provide in these zones of no-data.

HMA 8 m DEM

In 2017, the NASA National Snow and Ice Data Center (NSIDC) released the HMA 8 meter DEM datasets covering the eastern Pamir (Shean, 2017a, 2017b). These DEM datasets were extracted from along-track and cross-track stereoscopic imagery from DigitalGlobe satellites and were provided in strips. Each along-track DEM was acquired on a single date from two images acquired ~60 s apart and the cross-track DEMs were created from image pairs acquired <7 d apart with a spatial resolution of 8 m. In our study, we used 12 DEM strips with timestamps between 2015 and 2016 (Table S2). In order to have sufficient coverage over studied glaciers, some HMA DEMs acquired outside of the ablation season were also used. Before co-registration with SRTM, we resampled the HMA DEMs to 30 m as per the PRISM and SRTM DEMs.

DEM co-registration and biases omission

DEMs generated from different data sources may have inconsistent geolocations owing to sensor instabilities, method limitations, insufficient ground surveying conditions and different post-processing procedures (e.g. Nuth and Kääb, 2011). In this study, we co-registered the PRISM and HMA DEMs to the baseline SRTM DEM using the three-step correction framework of Nuth and Kääb (2011). Firstly, horizontal mismatches between each DEM pair were found and removed by iteratively shifting the slave DEM according to terrain slope and aspect differences. Secondly, elevation-dependent biases were adjusted using the linear or polynomial relationship between DEM elevations and the elevation differences. Finally, higher-order biases relating to satellite geometry (along/cross track) were checked in both the PRISM

https://doi.org/10.1017/jog.2020.54 Published online by Cambridge University Press

DEM and the HMA DEM. Examples of this procedure are shown in the Supplementary Figures S1 to S4. Mean DEM differences and the std dev. over off-glacier areas before and after co-registration processes are shown in Table S2.

SRTM DEM correction

Given the known penetration of C-band radar waves over snow- and glacier-covered terrain (Gardelle and others, 2012), the SRTM DEM was modified based on the identification of different snow- and ice-facies. Ice, firn and snow-covered areas were extracted by applying a threshold of 2.2 to the Landsat TM3/TM5 ratio (Kääb and others, 2012). After stretching the ratio (TM4 × TM2)/TM5 to values from 0 to 255, a threshold of 200 was used to discriminate firn and snow from clean ice (Kääb and others, 2012; King and others, 2017). Two Landsat ETM+ images acquired approximately coincident with the SRTM mission (Table S1) revealed little snow cover was present at this time, and the debris-covered glacier tongues were largely clear, unlike the heavy snow-cover conditions previously highlighted in Karakoram (Kääb and others, 2012). We therefore made no modification to the DEM for pixels corresponding with debris-covered ice. For all other areas, we adopted the penetration estimates of Zhang and others (2016a), who compared SRTM X-band and SRTM C-band data in a study area directly overlapping ours in the eastern Pamir, and we applied adjustments of +2.41 m over firn and snow areas and +0.79 m over clean ice areas.

Outlier filtering and gap filling

We differenced each pair of co-registered DEMs to derive glacier-wide maps of surface elevation change for the two periods of study (2000–09 and 2000–15/16). We discarded changes exceeding ±150 m for both glacierized and non-glacierized terrain as processing blunders and removed values >3 std dev. in off-glacier areas considering the elevation changes should not vary over stable terrain within one decade (Ragettli and others, 2016). Further visual inspection revealed the persistence of outliers in some accumulation areas, especially in the PRISM DEMs, as a consequence of image saturation and thus poor feature matching in the photogrammetric DEM extraction. For the accumulation zones, we therefore applied a threshold of ±30 m to the PRISM DEM-SRTM DEM elevation changes and ±45 m to the HMA DEM-SRTM DEM elevation changes assuming that accumulation areas did not experience continuous mass gain or loss of more than 3 m a^{-1}. It should be noted that the PRISM DEM-SRTM DEM generally has poor performance in snow-covered regions leading to bigger data gaps in glacier accumulation zones because of the low radiometric accuracy of the PRISM sensor (Saunier and others, 2010).

We filled the remaining data gaps over glacierized areas in order to calculate glacier-wide surface mass balances (Ragettli and others, 2016; King and others, 2017). The gaps were mostly located at high elevation and over steep slopes. For gaps in the HMA DEM-SRTM DEM difference data, we binned elevation change values per 100 m elevation band and used the median value from each band to fill the remaining gaps (Ragettli and others, 2016). To fill the gaps in the PRISM DEM-SRTM DEM difference data, we first used AW3D30 DEM-SRTM DEM difference data. We considered this approach to be more robust than filling with data from adjacent regions given that most of the gaps were in high-elevation zones where abrupt changes over the 5-year period are unlikely to have occurred, and therefore accurately represented by the AW3D30 composite dataset. We then filled any remaining small gaps (<5 × 5 grid cells) using the mean difference changes from surrounding cells.

Glacier delineation and identification of surge-type glaciers

We downloaded unmodified Randolph Glacier Inventory (RGI) version 6.0 (RGI Consortium, 2017) outlines and manually adjusted them to delineate ice extents in 2000, as close to the HMA DEM acquisition dates as cloud and snow-free Landsat ETM+ and OLI images would allow (Table S1). Fine resolution Google Earth images were also used to support glacial boundary identification. Digitizing glacier outlines manually carries with it an element of uncertainty (Hall and others, 2003; Kutuzov and others, 2019). Therefore, we measured the associated uncertainty using the method suggested by Paul and others (2013). We repeatedly digitized four glaciers with different sizes (Kn1, Ks5, Guerdaoban and Kekesayi) in our study area and calculated the accuracy from their std dev. The final accuracy is 1.0% for each individual, as all glaciers in our study have an area larger than 5 km^2 (Table S3).

We identified a glacier as surge-type if it underwent a sudden advance of its tongue within our study period, or exhibited specific and characteristic surface feature changes, such as looped or folded moraines or heavy surface crevassing (Meier and Post, 1969; Barrand and Murray, 2006). Landsat TM, ETM+ and OLI images from 1992 to 2020 were used to detect these changes (Table S1). DEM difference data were also used to identify surge events, characterized by a thinning of the upper part of a glacier coincident with a thickening of the lower part, suggesting a clear ice discharge from the reservoir zone to the receiving zone (Jiskoot, 2011; Bhambri and others, 2017). Additionally, we also used the results of surge inventories from previous studies (Holzer and others, 2015; Shangguan and others, 2016; Lv and others, 2019).

Calculation of glacier mass changes

For the purposes of this study, we restricted our analysis to 55 glaciers of area >5 km^2 with sufficient coverage of DEM difference data to ensure our remote-sensing analyses were robust (Table S3). Volume change (ΔV) for each glacier was calculated through Eqn (1):

$$\Delta V = \sum_{1}^{n} \Delta h_{\mathrm{pix}} \cdot A_{\mathrm{pix}}, \quad (1)$$

where n is the pixel number of elevation change map for each glacier, Δh_{pix} is the elevation change in each pixel, and A_{pix} is the area of each pixel given 900 m^2, as our DEMs share a spatial resolution of 30 m.

To convert volume change to mass balance, we applied a glacier-ice density (f_c) of 850 kg m^{-3} for calculating the water equivalent (w.e.) mass change and included an uncertainty (σ_f) of 60 kg m^{-3} in the density conversion (Huss, 2013; Zhang and others, 2016a). The mass-balance (MB) rate was defined by Eqn (2):

$$\mathrm{MB} = (\Delta V \cdot f_c)/(A \cdot \Delta t), \quad (2)$$

where A represents the glacier area (Table S3) and Δt is the period length between two DEMs used for co-registration.

Uncertainty assessment

Several sources of uncertainties contribute to the glacier mass-balance uncertainty including the elevation change uncertainty, the density uncertainty and the area uncertainty (Fischer and others, 2015; Kutuzov and others, 2019). We estimated the errors in elevation changes following the approach suggested by previous

https://doi.org/10.1017/jog.2020.54 Published online by Cambridge University Press

studies (Rolstad and others, 2009; Magnússon and others, 2016). Considering the influence of autocorrelation between DEMs, spatially correlated area (A_{corr}) is required in this approach, defined by Eqn (3):

$$A_{corr} = \pi \cdot L^2, \quad (3)$$

where L is the decorrelation length of 600 m for the PRISM DEMs and 400 m for the HMA DEMs (Bolch and others, 2011; Brun and others, 2017). As studied glaciers are larger than 5 km^2, $A > A_{corr}$ and the uncertainty of elevation change ($\sigma_{\Delta h}$) can be quantified using Eqn (4):

$$\sigma_{\Delta h} = SD\sqrt{A_{corr}/5A}, \quad (4)$$

where SD represents the std dev. of the elevation changes over the stable terrain.

The volume change uncertainty ($\sigma_{\Delta V}$) was obtained by Eqn (5):

$$\sigma_{\Delta V} = \sigma_{\Delta h} \cdot A. \quad (5)$$

With the errors discussed above, the uncertainty of the annual mass balance (σ_{MB}) was defined by Eqn (6):

$$\sigma_{MB} = \frac{\sqrt{(\Delta V \cdot \sigma_f/A)^2 + (\sigma_{\Delta V} \cdot f_c/A)^2 + (\Delta V \cdot f_c \cdot \sigma_A/A)^2}}{\Delta t}, \quad (6)$$

where f_c is the density conversion factor (0.85) with its uncertainty (σ_f) of 0.06 and σ_A is the area uncertainty which is 1.0% for each glacier.

Considering data voids can influence the error to some extent, we finally determined the total uncertainty through Eqn (7), as suggested by Zhou and others (2019a).

$$\sigma_{total} = \sigma_{MB}/R_{av}, \quad (7)$$

where R_{av} is the data coverage rate given in the Supplementary Tables S4 to S6.

We did not apply seasonality correction to glacier mass changes. As the eastern Pamir is considered to have relatively low annual precipitation (Shangguan and others, 2006), we assumed the decade-scale seasonal change to be negligible.

Results

Combined, the 55 glaciers within our sample showed a slightly positive mean mass balance of 0.06 ± 0.04 m w.e. a^{-1} between 2000 and 2015/16. In contrast, the 42 glaciers we have data for across our study region showed a slightly negative mean mass balance of −0.06 ± 0.16 m w.e. a^{-1} over the period 2000–09 (Table 1).

Muztag Ata had a positive mass balance with a mean value of 0.16 ± 0.03 m w.e. a^{-1} between 2000–15/16 (eight glaciers). The mean mass balance between 2000 and 2009 was 0.01 ± 0.12 m w.e. a^{-1} (six glaciers) although individual glacier mass-balance estimates varied substantially (Fig. 2, Table S4). Only Kuosikulake Glacier was identified as being of surge-type in the Muztag Ata. Holzer and others (2015) suggested this glacier was in an active surge phase until 2013.

The mass balance of 15 glaciers in the Kongur Tagh had a mean value of 0.17 ± 0.04 m w.e. a^{-1} between 2000 and 2015/16 (Fig. 3, Table S5). Most glaciers we studied were located on the western-facing slope and showed a positive mass balance; Ko9, one of our smallest studied glaciers, was the only glacier in a state of negative mass balance (−0.09 ± 0.04 m w.e. a^{-1}). Between 2000 and 2009, the ten glaciers we have data for were close to equilibrium (0.03 ± 0.12 m w.e. a^{-1}). We identified four surge-type glaciers in the Kongur Tagh: Kelayayilake, Ko6, Ko10 and Ko11. The surge of Kelayayilake had previously been reported by Shangguan and others (2016). It was the only surge-type glacier in the eastern Pamir recorded in RGI version 6.0.

Table 1. Average mass balances for glaciers in the eastern Pamir during two study periods: 2000–09 and 2000–15/16

Region	2000–09 (m w.e. a^{-1})	2000–15/16 (m w.e. a^{-1})
Muztag Ata	0.01 ± 0.12	0.16 ± 0.03
Kongur Tagh	0.03 ± 0.12	0.17 ± 0.04
Kingata (n-s combined)	−0.12 ± 0.19	−0.04 ± 0.04
Kingata (north)	−0.17 ± 0.22	−0.07 ± 0.04
Kingata (south)	−0.03 ± 0.15	0.02 ± 0.03
Eastern Pamir	**−0.06 ± 0.16**	**0.06 ± 0.04**

Eastern Pamir and its mass change values are bold type, as this row (the last row) represents the average mass balance condition of the entire region. The first five rows are only parts of the eastern Pamir.

Glaciers in the Kingata Mountains underwent a slight mass loss of −0.04 ± 0.04 m w.e. a^{-1} (23 glaciers) between 2000 and 2015/16 (Fig. 4, Table S6). The mean mass balance of glaciers on the northern slopes was −0.07 ± 0.04 m w.e. a^{-1}. However, glaciers on the southern slopes had a slight mass gain of 0.02 ± 0.03 m w.e. a^{-1}. Glaciers in the Kingata Mountains experienced more negative mass changes between 2000 and 2009: the mean value of 26 glaciers was −0.12 ± 0.19 m w.e. a^{-1}. North flowing glaciers had a mean mass balance of −0.17 ± 0.22 m w.e. a^{-1} and south flowing glaciers a mean mass balance of −0.03 ± 0.15 m w.e. a^{-1}. The Kingata Mountains had the largest number (15) of surge-type glaciers in the eastern Pamir. We identified three further surge-type glaciers not captured in the inventory of Lv and others (2019).

The subtly different mass balance of glaciers in different subregions of our study area indicates that the transition boundary from positive to negative mass balances lies at the northern end of Kongur Tagh (Fig. 1). Mass gains are dominant in the Kongur Tagh and Muztag Ata and mass losses prevail in the Kingata Mountains. However, the mass balances for all sub-regions are increasingly positive when comparing 2000–09 to 2000–15/16 (Fig. 5).

Of the 20 surge-type glaciers we identified in the eastern Pamir, 14 have been previously identified (Holzer and others, 2015; Shangguan and others, 2016; Lv and others, 2019; Table S7). Six glaciers were classified as surge-type for the first time; three of these were located in the Kongur Tagh and three were located in the Kingata Mountains. These interpretations were made based on the geodetic data, which showed discrete zones of ice discharge or recharge over our study period (Figs 3, 4; Table S7). It is possible that other surge-type glaciers exist within our dataset, but did not show morphological or geodetic evidence of surging during our analysis.

The coverage of HMA DEMs allowed for the derivation of the geodetic mass balance of 15 surge-type glaciers (Tables S4 to S6). Between 2000 and 2015/16, these glaciers had a slightly lower average mass balance (0.02 ± 0.03 m w.e. a^{-1}) than the remaining 31 non-surge type (0.08 ± 0.04 m w.e. a^{-1}). In the Kingata Mountains, where 11 out of the 15 surging glaciers are located, the average mass balances of the surge- and non-surge-type glaciers were identical (−0.03 ± 0.03 and −0.03 ± 0.04 m w.e. a^{-1}, respectively).

Discussion

Spatial and temporal variability in mass loss

Our data show that since the start of the 21st century, mass balance in the eastern Pamir has experienced a transition from a

https://doi.org/10.1017/jog.2020.54 Published online by Cambridge University Press

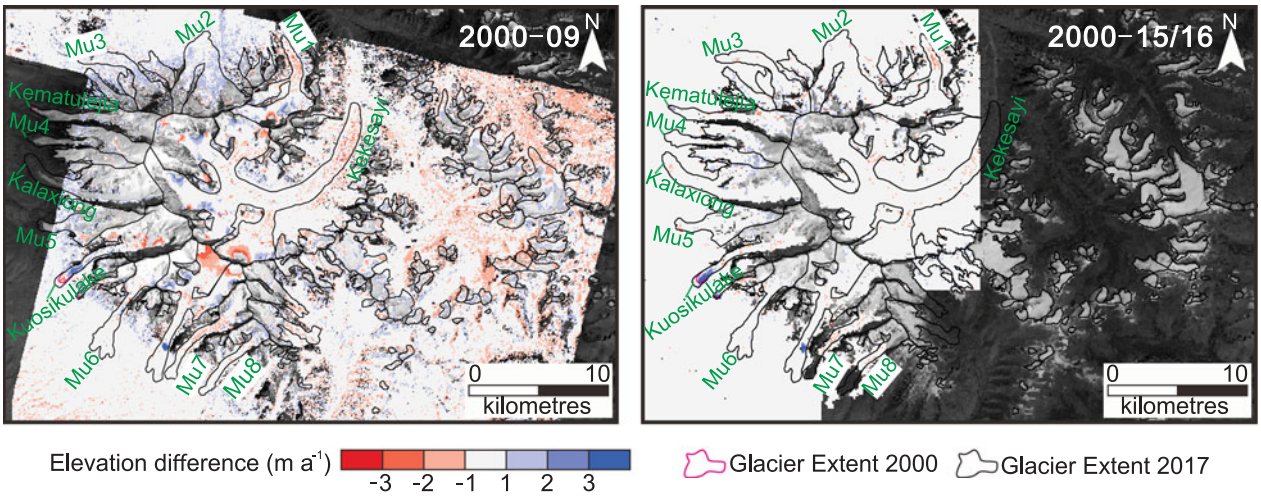


Fig. 2. Surface elevation change over Muztag Ata (a) between 2000 and 2009 and (b) between 2000 and 2015/16. The background is a Landsat OLI band 8 panchromatic image on 9 September 2017.

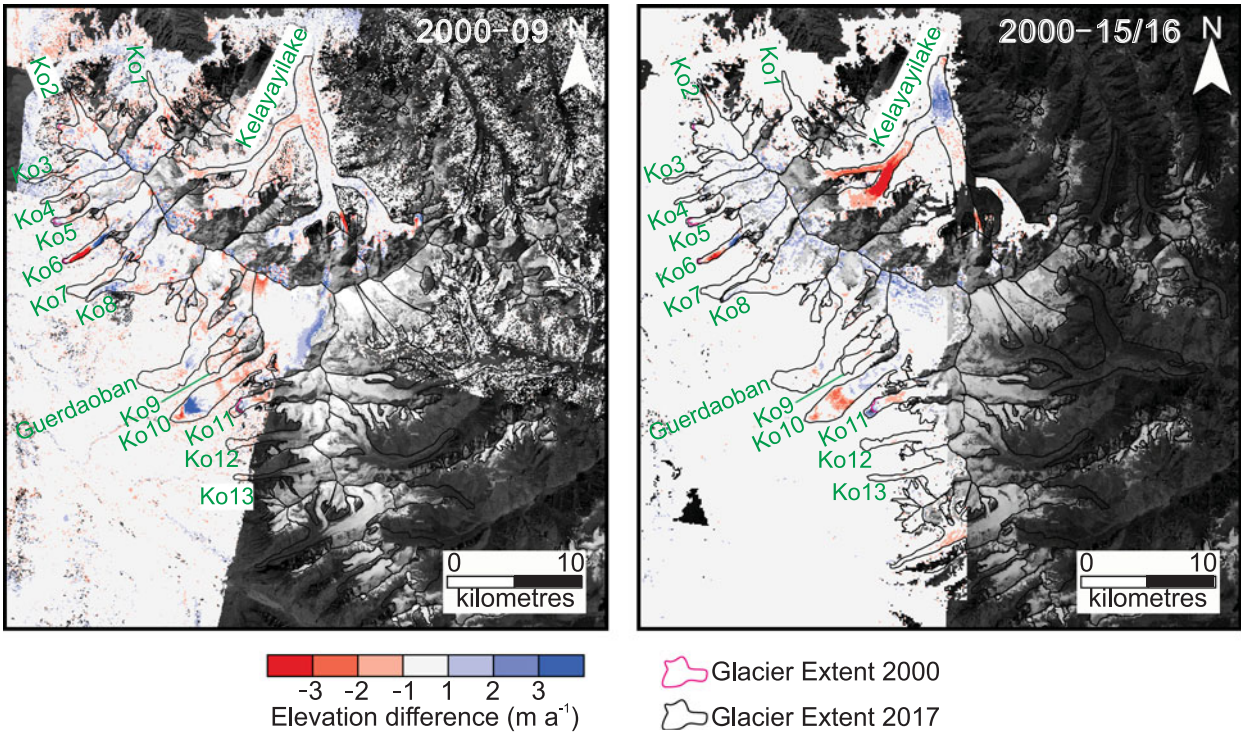


Fig. 3. Surface elevation change over Kongur Tagh (a) between 2000 and 2009 and (b) between 2000 and 2015/16. The background is a Landsat OLI band 8 panchromatic image on 9 September 2017.

marginal signal of mass loss (-0.06 ± 0.16 m w.e. a^{-1}) in 2000–09 to an equally marginal mass gain (0.06 ± 0.04 m w.e. a^{-1}) in 2000–15/16, with sub-regions showing temporally homogeneous and spatially consistent behavior (Table 1). These results are closely in line with the regional mass balance of 0.04 ± 0.06 m w.e. a^{-1} found by Shean and others (2020) over a similar period (2000–2018). This signal of equilibrium (and in places positive mass balance) in the eastern Pamir was already confirmed to extend from the Karakoram (Brun and others, 2017; Treichler and others, 2019). We find that mass changes in the Muztag Ata varied from 0.01 ± 0.12 m w.e. a^{-1} in 2000–09 to 0.16 ± 0.03 m w.e. a^{-1} in 2000–15/16 (Table 1). These results are largely in line with previous studies that observed mass gains of 0.04 ± 0.45 m w.e. a^{-1} (2000–09) and 0.04 ± 0.27 m w.e. a^{-1} (2000–13) (Holzer and others, 2015) and a positive elevation change of 0.17 ± 0.15 m a^{-1} (2003–2009) (Gardner and others, 2013). In-situ measurements of the Muztag Ata Glacier (a small glacier located between Mu5 and Kalaxiong in our study) also confirmed a 0.25 m w.e. a^{-1} mass gain from 2005/06 to 2009/10 (Yao and others, 2012).

In our study, glaciers in the Kongur Tagh show slightly positive mass balances of 0.03 ± 0.12 m w.e. a^{-1} in 2000–09 and 0.17 ± 0.04 m w.e. a^{-1} in 2000–15/16 (Table 1). Zhang and others (2016a) reported a slightly negative mass balance of -0.16 ± 0.25 m w.e. a^{-1} from 2000 to 2013/14 in this same region. However, it should be noted that most of the glaciers sampled in their study were eastern- and northern-facing. As most of our studied glaciers are located on the western slope, we suggest they may capture a disproportionate amount of the incoming

https://doi.org/10.1017/jog.2020.54 Published online by Cambridge University Press

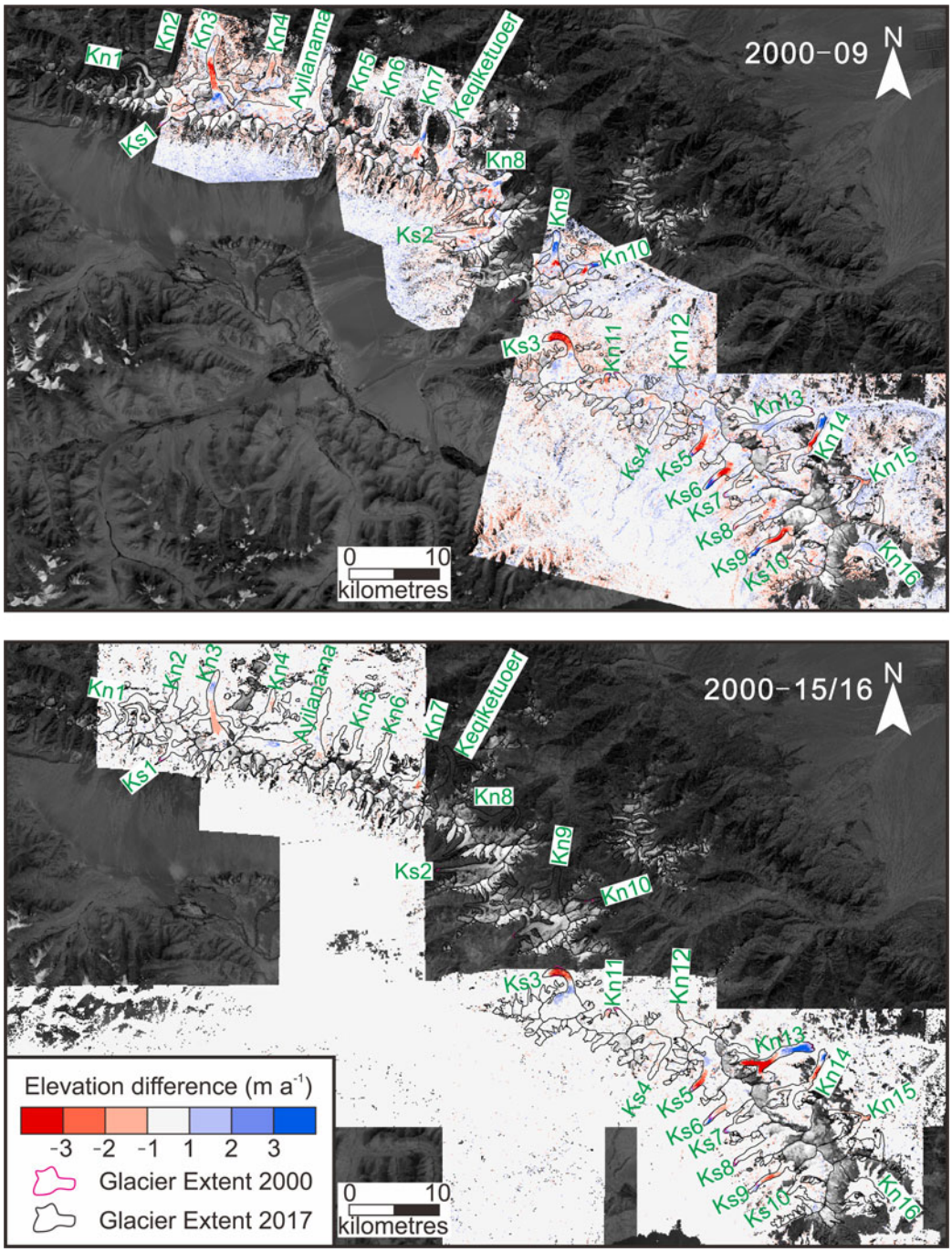


Fig. 4. Surface elevation change over Kingata Mountains (a) between 2000 and 2009 and (b) between 2000 and 2015/16. The background is a Landsat OLI band 8 panchromatic image on 9 September 2017.

westerly precipitation, accounting for this disparity in the results. Yao and others (2012) determined that increasing precipitation from the westerly wind resulted in the positive balance (0.25 m w.e. a^{-1}) of the Muztag Ata Glacier during 2005/06–2009/10. Lv and others (2019) also suggested glaciers on the southern wind-facing slope of Kingata Mountains have the potential to capture more precipitation than those to the north.

Glaciers in the Kingata Mountains were in negative mass balance across both our study periods, but became more positive toward the present day (from -0.12 ± 0.19 m w.e. a^{-1} in 2000–09 to -0.04 ± 0.04 m w.e. a^{-1} in 2000–15/16). The mean mass balance of glaciers on southern-facing slopes displayed a slight mass gain of 0.02 ± 0.03 m w.e. a^{-1} between 2000 and 2015/16 (Table 1). These data correlate well with a previously reported acceleration in glacier velocity of glaciers located on the southern slopes of the Kingata Mountains (Lv and others, 2019) detected over the periods 1999–2002 and 2013–16.

The spatial distribution of positive (Muztag Ata and Kongur Tagh) and negative (Kingata Mountains) mass-balance estimates we have derived suggests that the eastern Pamir may be the location of a transition zone of glacier fluctuations. The transition point appears to coincide with the Gez River (Fig. 1), which runs along a major fault separating two primary stratigraphic units in the region (Thiede and others, 2013). The topography and the relief differ notably between these two units (Fig. 5). Glaciers in the Kingata Mountains have a mean median elevation of 4913 m a.s.l., while glaciers in the Kongur Tagh and Muztag Ata share mean median elevations of 5662 and 5571 m a.s.l., respectively (Table S3). The distribution of precipitation is somewhat complicated by the extreme relief here and can vary

https://doi.org/10.1017/jog.2020.54 Published online by Cambridge University Press

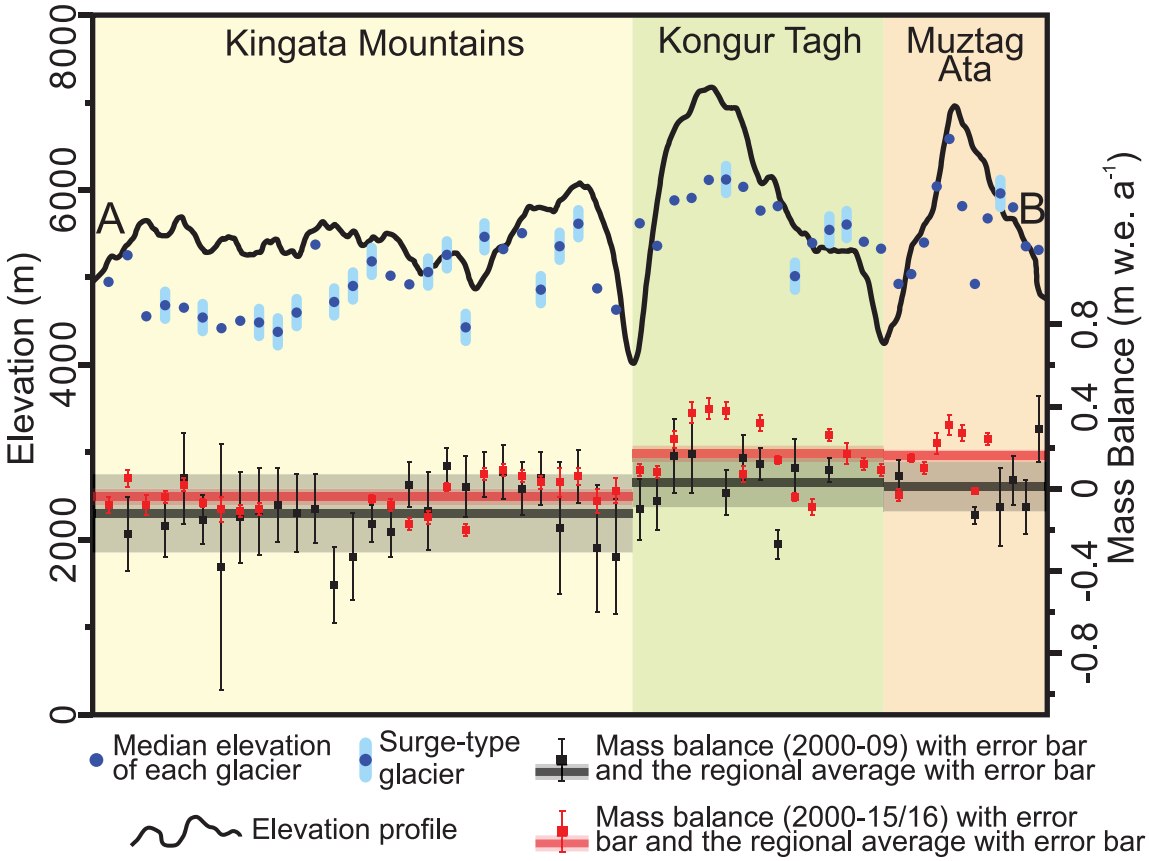


Fig. 5. Elevation profile with median elevation and mass balance of each studied glacier along the profile. The orbit of the elevation profile A-B is shown in Figure 1.

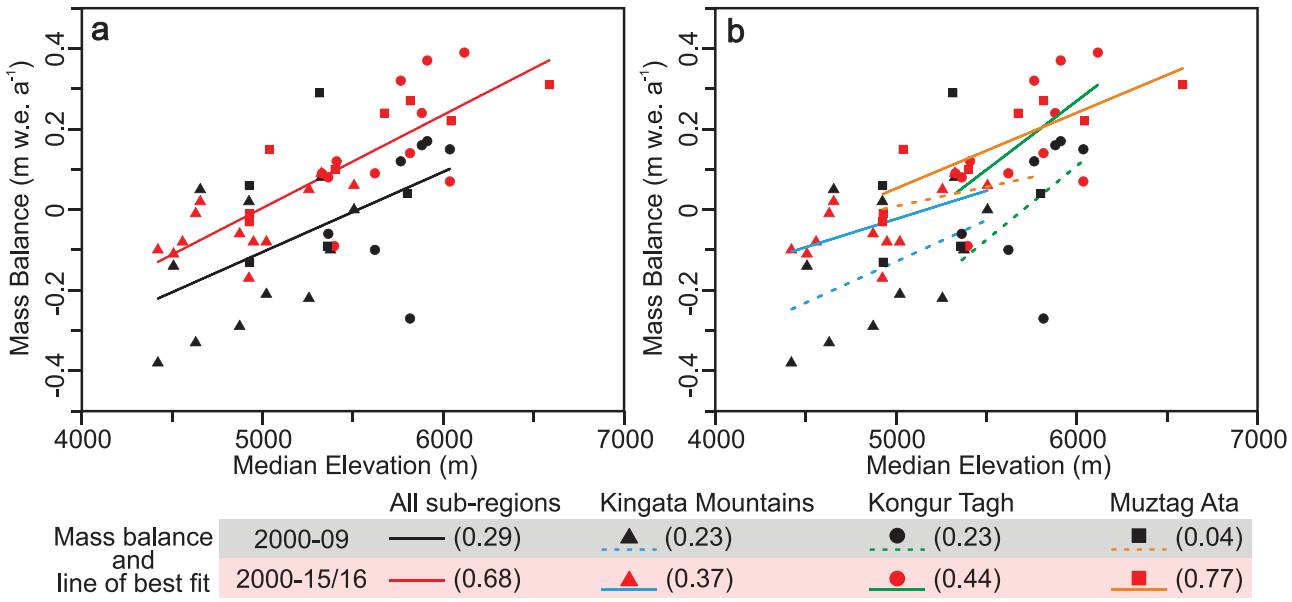


Fig. 6. The relationship between mass balance and median elevation of each non-surge-type glacier in the eastern Pamir. The lines of best fit for all sub-regions (a) and each region (b) during the two studied periods are shown. R^2 values for these lines are given in brackets.

considerably over small spatial scales (Anders and others, 2006). However, there does appear to be a clear orographic control on mass balance across the region.

These observations indicate that catchment topography plays an important role in determining mass-balance characteristics. Basing on a relatively strong relationship ($R^2 = 0.68$), mass balances increased by 0.23 m w.e. a^{-1} for every 1000 m in median elevation over the period 2000–2015/16 (Fig. 6a). Although the relationship between mass balance and topography is complex, and certainly the availability of ice avalanche material will play a role on an individual glacier scale, we suggest that glaciers located at higher elevations have generally been able to capture

https://doi.org/10.1017/jog.2020.54 Published online by Cambridge University Press

more solid precipitation than those at lower elevations, and have subsequently lost less to sublimation and melt (Stigter and others, 2018).

Similar patterns are replicated within individual ranges (Fig. 6b), but here local-scale controls on mass balance become more apparent. There is a noticeably steeper mass-balance gradient for the Kongur Tagh, but the elevation range for the glaciers is narrow, so variability induced by shading, slope and exposure, for example, is exaggerated ($R^2 = 0.44$ for 2000–2015/16). In the Kingata Mountains ($R^2 = 0.37$), there is a clear pattern of higher mass gain to the south, and lower mass gain to the north (Table 1), and the variability can be linked to the visibly more extensive accumulation areas feeding glaciers to the south when compared to those to the north (Fig. 1). The relationship between catchment topography and mass balance is in fact strongest in the Muztag Ata ($R^2 = 0.77$), where relief is extreme (Fig. 5), but most glaciers drain to the west of the divide and are largely consistent in size and surface characteristics (Fig. 1). Our conclusion then is that catchment topography, both on a regional and local scale, plays an important role in controlling these mass-balance patterns.

Mass balance of surge-type glaciers

Compared to more than 60 surging glaciers in the central Pamir (Kotlyakov and others, 2017), we found 20 surge-type glaciers in the eastern Pamir. Fifteen of these are located in the Kingata Mountains, four are in the Kongur Tagh, and one is located in the Muztag Ata (Table S7).

Despite key advances in recent years in characterizing surge dynamics (Quincey and others, 2011), identifying the climatic and geometric controls on surge-type glacier distribution (Sevestre and Benn, 2015), and an increasing number of regional mass-balance estimates that incorporate both surge-type and non-surge-type glaciers (Berthier and others, 2019), the links between climate and surging are still relatively poorly understood (Kochtitzky and others, 2020). There is clear consensus that surging is predominantly regulated by internal glacier dynamics rather than external climate forcing, yet there may be connections to mass balance, at least at a point if not glacier-wide (Eisen and others, 2001; Flowers and others, 2011). Several studies have evidenced that during the active stage of surging, glaciers can undergo enhanced ablation, as large volumes of ice are transported to lower and warmer elevations (Aðalgeirsdóttir and others, 2005; Kochtitzky and others, 2019), but over decadal timescales, these fluctuations are not captured (Gardelle and others, 2013).

The mass balances of surge-type glaciers should therefore be analyzed carefully (Bhambri and others, 2017). Those presented here show both spatial and temporal variability, but, consistent with other studies, there is evidence of a subtle pattern of fluctuation before, during and after the observed surge events. For example, both Kelayayilake and Ko10 glaciers surged in 2015 and showed positive mass balance before the surges, but entered a period of more negative mass balance during and after the surge events, contrasting with the pattern of mass gain for other glaciers on the southern slope of Kingata Mountains (e.g. Ks6 and Ks10). Glaciers Kn14 and Kn13 also experienced several years of markedly more negative mass balance following their surge events. Glacier Ko6 surged prior to 2000, and showed negative mass balance until 2009, but then transitioned to positive mass balance until 2016, coincident with a period of reservoir recharge after the surge event.

The mass-balance differences of surge-type (0.02 ± 0.03 m w.e. a^{-1}) and non-surge-type glaciers (0.08 ± 0.04 m w.e. a^{-1}) in 2000–15/16 highlighted in our results are within the uncertainty of our data and are not statistically significant, in line with previous studies (Gardelle and others, 2013). The mean annual mass budget excluding surge-type glaciers was -0.06 ± 0.04 m w.e. a^{-1} (-0.07 ± 0.04 m w.e. a^{-1} with surge-type included) on the northern slopes of Kingata Mountains and 0.01 ± 0.03 m w.e. a^{-1} (0.02 ± 0.03 m w.e. a^{-1} with surge-type included) on the southern slopes. Kongur Tagh also showed very similar mass balances without (0.17 ± 0.04 m w.e. a^{-1}) and with (0.17 ± 0.04 m w.e. a^{-1}) surging glaciers included. In the central Pamir, the mean mass balances of surge-type glaciers (0.03 ± 0.14 m w.e. a^{-1}) and non-surge-type glaciers (-0.05 ± 0.28 m w.e. a^{-1}) between 1975 and 1999 were also not significantly different (Zhou and others, 2019b). We therefore suggest that the inclusion of surge-type glaciers in regional assessments derived over a decadal timescale may not impact significantly on the calculated mass budget, but that when assessing geodetic mass balance on an individual glacier scale, due consideration should be given to where that glacier is within its own surge cycle (Kochtitzky and others, 2019).

Glacier mass-balance uncertainty

Although we accounted for all possible methodological uncertainties in our data, there remain some elements that cannot be explicitly quantified. Common issues in studies of geodetic mass balance include the biases introduced by data voids (Tables S4 to S6) or anomalous glacier surface elevation data resulting from low image contrast, particularly in glacier accumulation zones (McNabb and others, 2019). Similarly, the penetration of C-band radar waves into snow and ice has been shown to cause the underestimation of glacier surface elevation change by as much as 20% at a regional scale if left uncorrected (Gardelle and others, 2012; Vijay and Braun, 2016). Large fluctuations in glacier reference areas between DEM acquisitions may also introduce systematic errors (Zemp and others, 2013), as can the spatial autocorrelation of elevation differences (Rolstad and others, 2009) and the spatially variable density of ice and firn (Huss, 2013).

Our use of the C-band SRTM DEM and ALOS PRISM images of relatively low radiometric resolution, and the inclusion of surge-type glaciers that have undergone dramatic morphological changes between one DEM acquisition and the next, makes biases relating to surface penetration, DEM blunders and spatially variable ice density most pertinent in our study.

The availability of Landsat ETM+ scenes close to the acquisition date of the SRTM over our study area allowed for the application of penetration corrections depending on glacier surface conditions. We were therefore able to account for the spatial (elevation-dependent) variability in penetration (Vijay and Braun, 2016) across our study area. We carefully selected the threshold to remove erroneous PRISM DEM-SRTM DEM difference data over glacier accumulation zones, where the magnitude of elevation change is expected to be low. Similar elevation-dependent filtering has been successfully applied in other studies using low radiometric resolution imagery (Pieczonka and Bolch, 2015) where more typical, statistical filtering (e.g. Gardelle and others, 2013) may not be sufficient.

Ice density conversion factors have been given specific attention in the literature in recent years (Huss, 2013), but still require some element of estimation or assumption. In our study, the use of a single factor is further complicated by the fact that during and after a surge event, the glacier surface is completely reorganized such that with the development of deep crevassing, the ice surface is effectively more porous. It may be, therefore, that for surge-type glaciers in particular, our conversion factor represents an overestimate of ice density. Ultimately, however, the close agreement of our mass-balance estimates with those of other studies, in particular those not involving the SRTM (e.g. Shean and others, 2020), suggests our results are robust.

https://doi.org/10.1017/jog.2020.54 Published online by Cambridge University Press

Conclusions

Using three DEM datasets, the SRTM DEM, the NASA HMA DEM and individual DEMs extracted from ALOS PRISM optical imagery during the intervening period, we reconstructed the mass-balance conditions of glaciers in the eastern Pamir for two epochs: 2000–09 and 2000–15/16. Our data confirm that the eastern Pamir is a transition zone from positive to negative mass balance with the boundary located at the north end of Kongur Tagh, and coincident with the Gez River, which separates two major stratigraphic units of contrasting topography. Overall, glaciers in the Muztag Ata and Kongur Tagh experienced mass gain and glaciers in the Kingata Mountains experienced mass loss during the first part of the 21st century, while almost all glaciers gained more mass (or lost less mass) through time. Individual catchment topography plays a strong role in determining glacier mass-balance characteristics, with those glaciers located at higher elevations showing, on average, more positive mass balance than those situated at lower elevations. Finally, we find that over broad areas and decadal timescales, the impact of including surge-type glaciers on regional mass budget calculations is statistically insignificant, but that during and immediately after surge events, individual glaciers may enter periods of negative mass balance as a consequence of enhanced ablation.

Supplementary material. The supplementary material for this article can be found at https://doi.org/10.1017/jog.2020.54

Acknowledgements. This research was supported by the Key Research Program of Frontier Sciences CAS [QYZDY-SSW-DQC026] and the National Natural Science Foundation of China [41590853]. SRTM DEM and NASA HMA DEM data were sourced from NASA Earthdata (https://earthdata.nasa.gov/), and the ALOS Global Digital Surface Model (AW3D30) was sourced from JAXA (https://www.eorc.jaxa.jp/ALOS/en/aw3d30/index.htm). ALOS PRISM level-1B1 products were ordered from http://en.alos-pasco.com/alos/prism/ under a 4th ALOS RA data grant awarded to Quincey (PI No. 1008). Landsat-7 and Landsat-8 images can be freely downloaded from http://glovis.usgs.gov. Randolph Glacier Inventory data were acquired from Global Land Ice Measurements from Space (GLIMS) (RGI Consortium, 2017). Lv acknowledges program B for outstanding PhD candidates of Nanjing University and the support from the Chinese Scholarship Council (CSC) for studying at the University of Leeds. We also thank Rakesh Bhambri, Hester Jiskoot and three anonymous reviewers for their supportive comments on this paper.

Conflict of interest. The authors declare that they have no conflict of interest.

References

Aðalgeirsdóttir G, Björnsson H, Pálsson F and Magnússon E (2005) Analyses of a surging outlet glacier of Vatnajökull ice cap, Iceland. *Annals of Glaciology* **42**, 23–28. doi: 10.3189/ 172756405781812934.

Anders AM and 5 others (2006) Spatial patterns of precipitation and topography in the Himalaya. In Willett SD, Hovius N, Brandon MT and Fisher D (eds), Tectonics, Climate, and Landscape Evolution: Geological Society of America Special Paper. 398, pp. 39–53. doi: 10.1130/2006.2398(03).

Barrand NE and Murray T (2006) Multivariate controls on the incidence of glacier surging in the Karakoram Himalaya. *Arctic, Antarctic, and Alpine Research* **38**(4), 489–498. doi: 10.1657/1523-0430(2006)38[489:mcotio]2.0.co;2.

Berthier E and Brun F (2019) Karakoram geodetic glacier mass balances between 2008 and 2016: persistence of the anomaly and influence of a large rock avalanche on Siachen Glacier. *Journal of Glaciology* **65**(251), 494–507. doi: 10.1017/jog.2019.32.

Bhambri R, Hewitt K, Kawishwar P and Pratap B (2017) Surge-type and surge-modified glaciers in the Karakoram. *Scientific Reports* **7**(1), 1–14. doi: 10.1038/s41598-017-15473-8.

Bolch T and 11 others (2012) The state and fate of Himalayan glaciers. *Science* **336**(6079), 310. doi: 10.1126/science.1215828.

Bolch T, Pieczonka T and Benn DI (2011) Multi-decadal mass loss of glaciers in the Everest area (Nepal Himalaya) derived from stereo imagery. *The Cryosphere* **5**(2), 349–358. doi: 10.5194/tc-5-349-2011.

Brun F, Berthier E, Wagnon P, Kääb A and Treichler D (2017) A spatially resolved estimate of High Mountain Asia glacier mass balances from 2000 to 2016. *Nature Geoscience* **10**, 668. doi: 10.1038/ngeo2999.

Eisen O, Harrison WD and Raymond CF (2001) The surges of Variegated Glacier, Alaska, USA, and their connection to climate and mass balance. *Journal of Glaciology* **47**(158), 351–358. doi: 10.3189/172756501781832179.

Farinotti D, Immerzeel W, de Kok R, Quincey DJ and Dehecq A (2020) Manifestations and mechanisms of the Karakoram glacier Anomaly. *Nature Geoscience* **13**(1), 8–16. doi: 10.1038/s41561-019-0513-5.

Farr TG and 17 others (2007) The shuttle radar topography mission. *Reviews of Geophysics* **45**(2), RG2004. doi: 10.1029/2005RG000183.

Fischer M, Huss M and Hölzle M (2015) Surface elevation and mass changes of all Swiss glaciers 1980–2010. *The Cryosphere* **9**(2), 525–540. doi: 10.5194/tc-9-525-2015.

Flowers GE, Roux N, Pimentel S and Schoof CG (2011) Present dynamics and future prognosis of a slowly surging glacier. *The Cryosphere* **5**, 299–313. doi: 10.5194/tc-5-299-2011.

Gardelle J, Berthier E and Arnaud Y (2012) Impact of resolution and radar penetration on glacier elevation changes computed from DEM differencing. *Journal of Glaciology* **58**, 419–422. doi: 10.3189/2012JoG11J175.

Gardelle J, Berthier E, Arnaud Y and Kääb A (2013) Region-wide glacier mass balances over the Pamir-Karakoram-Himalaya during 1999-2011. *The Cryosphere* **7**(4), 1263–1286. doi: 10.5194/tc-7-1263-2013.

Gardner AS and 15 others (2013) A reconciled estimate of glacier contributions to sea level rise: 2003 to 2009. *Science* **340**(6134), 852. doi: 10.1126/science.1234532.

Hall DK, Bahr KJ, Shoener W, Bindschadler RA and Chien JYL (2003) Consideration of the errors inherent in mapping historical glacier positions in Austria from the ground and space. *Remote Sensing of Environment* **86**, 566–577. doi: 10.1016/S0034-4257(03)00134-2.

Holzer N and 5 others (2015) Four decades of glacier variations at Muztagh Ata (eastern Pamir): a multi-sensor study including Hexagon KH-9 and Pléiades data. *The Cryosphere* **9**(6), 2071–2088. doi: 10.5194/tc-9-2071-2015.

Huss M (2013) Density assumptions for converting geodetic glacier volume change to mass change. *The Cryosphere* **7**(3), 877–887. doi: 10.5194/tc-7-877-2013.

IPCC (2019) IPCC Special Report on the Ocean and Cryosphere in a Changing Climate. Available at https://www.ipcc.ch/srocc/ (accessed 15 February 2020).

Jiskoot H (2011) Glacier surging. In Singh VP, Singh P and Haritashya UK (eds), *Encyclopaedia of Snow, Ice and Glaciers*. Heidelberg: Springer, pp. 415–428. doi: 10.1007/978-90-481-2642-2_559.

Kääb A, Berthier E, Nuth C, Gardelle J and Arnaud Y (2012) Contrasting patterns of early twenty-first-century glacier mass change in the Himalayas. *Nature* **488**, 495. doi: 10.1038/nature11324.

Kääb A, Treichler D, Nuth C and Berthier E (2015) Brief communication: contending estimates of 2003–2008 glacier mass balance over the Pamir–Karakoram–Himalaya. *The Cryosphere* **9**(2), 557–564. doi: 10.5194/tc-9-557-2015.

King O, Quincey DJ, Carrivick JL and Rowan AV (2017) Spatial variability in mass loss of glaciers in the Everest region, central Himalayas, between 2000 and 2015. *The Cryosphere* **11**(1), 407–426. doi: 10.5194/tc-11-407-2017.

Kochtitzky W and 6 others (2019) Terminus advance, kinematics and mass redistribution during eight surges of Donjek Glacier, St. Elias Range, Canada, 1935 to 2016. *Journal of Glaciology* **65**(252), 565–579. doi: 10.1017/jog.2019.34.

Kochtitzky W and 9 others (2020) Climate and surging of Donjek Glacier, Yukon, Canada. *Arctic, Antarctic, and Alpine Research* **52**(1), 264–280. doi: 10.1080/15230430.2020.1744397.

Kotlyakov VM, Osipova GB and Tsvetkov DG (2017) Monitoring surging glaciers of the Pamirs, Central Asia, from space. *Annals of Glaciology* **48**, 125–134. doi: 10.3189/172756408784700608.

Kutuzov S, Lavrentiev I, Smirnov A, Nosenko G and Petrakov D (2019) Volume changes of Elbrus Glaciers from 1997 to 2017. *Frontiers in Earth Science* **7**, 153. doi: 10.3389/feart.2019.00153.

Lin H, Li G, Cuo L, Hooper A and Ye Q (2017) A decreasing glacier mass balance gradient from the edge of the Upper Tarim Basin to the Karakoram during 2000–2014. *Scientific Reports* **7**(1), 6712. doi: 10.1038/s41598-017-07133-8.

Liu S and 7 others (2006) Glacier retreat as a result of climate warming and increased precipitation in the Tarim river basin, northwest China. *Annals of Glaciology* **43**, 91–96. doi: 10.3189/172756406781812168.

Lv M and 7 others (2016) A rapid glacier surge on Mount Tobe Feng, western China, 2015. *Journal of Glaciology* **62**(232), 407–409. doi: 10.1017/jog.2016.42.

Lv M and 7 others (2019) Characterizing the behaviour of surge- and non-surge-type glaciers in the Kingata Mountains, eastern Pamir, from 1999 to 2016. *The Cryosphere* **13**(1), 219–236. doi: 10.5194/tc-13-219-2019.

Magnússon E, Belart JMC, Pálsson F, Ágústsson H and Crochet P (2016) Geodetic mass balance record with rigorous uncertainty estimates deduced from aerial photographs and lidar data – case study from Drangajökull ice cap, NW Iceland. *The Cryosphere* **10**, 159–177. doi: 10.5194/tc-10-159-2016.

Maurer JM, Schaefer JM, Rupper S and Corley A (2019) Acceleration of ice loss across the Himalayas over the past 40 years. *Science Advances* **5**(6), eaav7266. doi: 10.1126/sciadv.aav7266.

McNabb R, Nuth C, Kääb A and Girod L (2019) Sensitivity of glacier volume change estimation to DEM void interpolation. *The Cryosphere* **13**(3), 895–910. doi: 10.5194/tc-13-895-2019.

Meier MF and 7 others (2007) Glaciers dominate eustatic sea-level rise in the 21st century. *Science* **317**(5841), 1064. doi: 10.1126/science.1143906.

Meier MF and Post A (1969) What are glacier surges? *Canadian Journal of Earth Sciences* **6**(4), 807–817. doi:10.1139/e69-081.

Mölg N, Bolch T, Rastner P, Strozzi T and Paul F (2018) A consistent glacier inventory for Karakoram and Pamir derived from Landsat data: distribution of debris cover and mapping challenges. *Earth System Science Data* **10**, 1807–1827. doi: 10.5194/essd-10-1807-2018.

Nuth C and Kääb A (2011) Co-registration and bias corrections of satellite elevation data sets for quantifying glacier thickness change. *The Cryosphere* **5**(1), 271–290. doi: 10.5194/tc-5-271-2011.

Oerlemans J (1994) Quantifying global warming from the retreat of glaciers. *Science* **264**(5156), 243. doi: 10.1126/science.264.5156.243.

Paul F and 19 others (2013) On the accuracy of glacier outlines derived from remote-sensing data. *Annals of Glaciology* **54**, 171–182. doi: 10.3189/2013AoG63A296.

Pieczonka T and Bolch T (2015) Region-wide glacier mass budgets and area changes for the Central Tien Shan between ~1975 and 1999 using Hexagon KH-9 imagery. *Global and Planetary Change* **128**, 1–13. doi: 10.1016/j.gloplacha.2014.11.014.

Quincey DJ and 5 others (2011) Karakoram Glacier surge dynamics. *Geophysical Research Letters* **38**(18), L18504. doi: 10.1029/2011GL049004.

Ragettli S, Bolch T and Pellicciotti F (2016) Heterogeneous glacier thinning patterns over the last 40 years in Langtang Himal, Nepal. *The Cryosphere* **10** (5), 2075–2097. doi: 10.5194/tc-10-2075-2016.

RGI Consortium (2017) Randolph Glacier Inventory – A Dataset of Global Glacier Outlines: Version 6.0: Technical Report. Global Land Ice Measurements from Space, Colorado, USA. Digital Media. doi: 10.7265/N5-RGI-60.

Rignot E, Echelmeyer K and Krabill W (2001) Penetration depth of interferometric synthetic-aperture radar signals in snow and ice. *Geophysical Research Letters* **28**(18), 3501–3504. doi: 10.1029/2000GL012484.

Rolstad C, Haug T and Denby B (2009) Spatially integrated geodetic glacier mass balance and its uncertainty based on geostatistical analysis: application to the western Svartisen ice cap, Norway. *Journal of Glaciology* **55**(192), 666–680. doi: 10.3189/002214309789470950.

Saunier S and 7 others (2010) Radiometric, geometric, and image quality assessment of ALOS AVNIR-2 and PRISM sensors. *IEEE Transactions on Geoscience and Remote Sensing* **48**(10), 3855–3866. doi: 10.1109/TGRS.2010.2048714.

Seong YB, Owen LA, Yi C, Finkel RC and Schoenbohm L (2009) Geomorphology of anomalously high glaciated mountains at the northwestern end of Tibet: Muztag Ata and Kongur Shan. *Geomorphology* **103** (2), 227–250. doi: 10.1016/j.geomorph.2008.04.025.

Sevestre H and Benn DI (2015) Climatic and geometric controls on the global distribution of surge-type glaciers: implications for a unifying model of surging. *Journal of Glaciology* **61**(228), 646–662. doi: 10.3189/2015JoG14J136.

Shangguan D and 9 others (2006) Monitoring the glacier changes in the Muztag Ata and Konggur mountains, east Pamirs, based on Chinese Glacier Inventory and recent satellite imagery. *Annals of Glaciology* **43**, 79–85. doi: 10.3189/172756406781812393.

Shangguan D and 6 others (2016) Characterizing the May 2015 Karayaylak Glacier surge in the eastern Pamir Plateau using remote sensing. *Journal of Glaciology* **62**(235), 944–953. doi:10.1017/jog.2016.81.

Shean DE and 6 others (2016) An automated, open-source pipeline for mass production of digital elevation models (DEMs) from very-high-resolution commercial stereo satellite imagery. *ISPRS Journal of Photogrammetry and Remote Sensing* **116**, 101–117. doi: 10.1016/j.isprsjprs.2016.03.012.

Shean D (2017a) *High Mountain Asia 8-meter DEMs Derived from Along-track Optical Imagery, Version 1*. Boulder, Colorado, USA: NASA National Snow and Ice Data Center Distributed Active Archive Center. doi: 10.5067/GSACB044M4PK.

Shean D (2017b) *High Mountain Asia 8-meter DEMs Derived from Cross-track Optical Imagery, Version 1*. Boulder, Colorado, USA: NASA National Snow and Ice Data Center Distributed Active Archive Center. doi: 10.5067/0MCWJJH5ABYO.

Shean DE and 5 others (2020) A systematic, regional assessment of High Mountain Asia glacier mass balance. *Frontiers in Earth Science* **7**, 363. doi: 10.3389/feart.2019.00363.

Stigter EE and 6 others (2018) The importance of snow sublimation on a Himalayan Glacier. *Frontiers in Earth Science* **6**, 108. doi: 10.3389/feart.2018.00108.

Tadono T and 5 others (2014) Precise global DEM generation by ALOS PRISM. *ISPRS Annals of the Photogrammetry, Remote Sensing and Spatial Information Sciences* **2**, 71–76. doi: 10.5194/isprsannals-II-4-71-2014.

Tadono T, Shimada M, Murakami H and Takaku J (2009) Calibration of PRISM and AVNIR-2 Onboard ALOS 'Daichi'. *IEEE Transactions on Geoscience and Remote Sensing* **47**(12), 4042–4050. doi: 10.1109/TGRS.2009.2025270.

Thiede RC and 6 others (2013) Late Cenozoic extension and crustal doming in the India-Eurasia collision zone: new thermochronologic constraints from the NE Chinese Pamir. *Tectonics* **32**(3), 763–779. doi: 10.1002/tect.20050.

Tian L and 8 others (2006) Recent rapid warming trend revealed from the isotopic record in Muztagata ice core, eastern Pamirs. *Journal of Geophysical Research: Atmospheres* **111**(D13), D13103. doi: 10.1029/2005JD006249.

Treichler D, Kääb A, Salzmann N and Xu CY (2019) Recent glacier and lake changes in High Mountain Asia and their relation to precipitation changes. *The Cryosphere* **13**, 2977–3005. doi: 10.5194/tc-13-2977-2019.

Vijay S and Braun M (2016) Elevation change rates of glaciers in the Lahaul-Spiti (Western Himalaya, India) during 2000–2012 and 2012–2013. *Remote Sensing* **8**(12), 1038. doi: 10.3390/rs8121038.

Yao T and 14 others (2012) Different glacier status with atmospheric circulations in Tibetan Plateau and surroundings. *Nature Climate Change* **2**, 663. doi: 10.1038/nclimate1580.

Zemp M and 16 others (2013) Reanalysing glacier mass balance measurement series. *The Cryosphere* **7**, 1227–1245. doi: 10.5194/tc-7-1227-2013.

Zemp M and 38 others (2017) Historically unprecedented global glacier decline in the early 21st century. *Journal of Glaciology* **61**(228), 745–762. doi: 10.3189/2015JoG15J017.

Zhang X (1980) Recent variations in the glacial termini along the Karakoram Highway. *Acta Geographica Sinica* **47**(2), 149–160. doi: 10.11821/xb198002006.

Zhang Z and 6 others (2016a) Mass change of glaciers in Muztag Ata-Kongur Tagh, Eastern Pamir, China from 1971/76 to 2013/14 as derived from remote sensing data. *PLoS ONE* **11**(1), e0147327. doi: 10.1371/journal.pone.0147327.

Zhang Z and 5 others (2016b) Glacier changes since the early 1960s, eastern Pamir, China. *Journal of Mountain Science* **13**(2), 276–291. doi: 10.1007/s11629-014-3172-4.

Zhou Y and 5 others (2019a) Quantifying glacier mass change and its contribution to lake growths in central Kunlun during 2000–2015 from multi-source remote sensing data. *Journal of Hydrology* **570**, 38–50. doi: 10.1016/j.jhydrol.2019.01.007.

Zhou Y, Li Z, Li J, Zhao R and Ding X (2019b) Geodetic glacier mass balance (1975–1999) in the central Pamir using the SRTM DEM and KH-9 imagery. *Journal of Glaciology* **65**(250), 309–320. doi: 10.1017/jog.2019.8.

https://doi.org/10.1017/jog.2020.54 Published online by Cambridge University Press